Silicalite-1 Growth from Clear Solution: Effect of the Structure-Directing Agent on Growth Kinetics

Chil-Hung Cheng and Daniel F. Shantz*

Department of Chemical Engineering, Texas A&M University, College Station, Texas 77843-3122

Received: February 10, 2005; In Final Form: May 3, 2005

Small-angle X-ray scattering (SAXS) has been used to quantify how perturbations of the tetrapropylammonium (TPA) cation structure affect the growth of silicalite-1 from clear solutions at 368 K. Alkyltripropylammonium ($RN(C_3H_7)_3{}^+OH^-$, R = Me, Et, Bu, and Pe), dialkyldipropylammonium ($R_2N(C_3H_7)_2{}^+OH^-$, R = Et and Bu), and bis-1,6-(tripropylammonium)hexamethylene dihydroxide (TPA-dimer) cations are used as structure-directing agents (SDAs) to synthesize silicalite-1 from clear solution mixtures comparable to those that have been previously investigated for the TPAOH mediated synthesis (i.e., 1 TEOS:0.36 TPAOH:20 H_2O, 368 K). All mixtures studied except those employing dialkyldipropylammonium cations lead to the formation of silicalite-1. The in-situ SAXS investigations show that TPA cations lead to the shortest reaction time as indicated by the observance of Bragg diffraction peaks (15∼16.5 h) and the largest particle growth rate (1.9 ± 0.1 nm/h). Substituting a propyl group of the TPA moiety with a different alkyl group significantly affects silicalite-1 nucleation and growth with the trend Bu > Et > Pe > Me. Synthesis mixtures containing the TPA-dimer also show a slower growth rate. All the solutions show a bimodal particle distribution throughout zeolite growth with the primary particle size being approximately 5 nm in all cases, independent of the SDA identity. Syntheses using diethyldipropylammonium hydroxide, dibutyldipropylammonium hydroxide, and 4,4′-trimethylenebis(1-methyl-1-hexyl-piperidinium) dihydroxide as the SDA do not result in silicalite-1 formation, showing that the nucleation of silicalite-1 from clear solution at 368 K is sensitive to the SDA geometry.

Introduction

Zeolites are an important class of microporous solids widely used in heterogeneous catalysis, the adsorption and separation of gases, and ion-exchange operations.[1−7] This is due to their highly crystalline structures, uniformity of their pores, the resulting shape selectivity observed in separations and catalysis, and subsequently the correlation between their microstructure and macroscopic properties.[8−10] Given the importance of these materials knowing the details of their formation has been recognized as the origin to manipulating zeolite properties for various applications and has been an intensely investigated topic. The growth of silicalite-1 (pure-silica ZSM-5) has been extensively studied[11−44] partly because of its ease of synthesis but also because MFI materials possess unique catalytic and adsorption properties. The MFI structure is comprised of straight 10 membered silicate-ring channels and zigzag sinusoidal 10 membered ring channels which intersect, and the pore diameters are approximately 5.5 Å.[45] The silicalite-1 synthesis is quite robust and can be made from either a gel phase[12−14,19,30,46] or a clear solution,[15−18,20,21,29,34−44] from which two types of nucleation mechanisms are proposed: heterogeneous and homogeneous nucleation. The growth of silicalite-1 from gel phases likely follows a heterogeneous nucleation pathway[30] and has been studied using methods including powder X-ray diffraction (PXRD), $^1H-^{29}Si$ CP MAS NMR, and small-angle X-ray scattering.[12−14,19,30,46]

During the past decade, syntheses of silicalite-1 from optically transparent mixtures of TEOS/TPAOH/water have been intensely studied by the zeolite science community.[15−18,20,26,27,29,31,34−44] The precursor solution can be easily prepared by mixing tetraethyl orthosilicate (TEOS), tetrapropylammonium hydroxide (TPAOH), and water. The low synthesis temperature (<368 K) and optically transparent nature of the initial solution facilitates in-situ studies, particularly those employing light scattering. This synthesis also enjoys the advantage that it is comprised of only three reagents. As such, this would appear to be as "simple" of a system as one could employ to form siliceous zeolites. These investigations have employed techniques including dynamic light scattering (DLS), calorimetry, small-angle X-ray scattering, and pH studies.[11,15,20,22,24,26,28,34−41,43,44] An ex-situ DLS investigation of silicalite-1 syntheses at 373 K shows that discrete colloidal particles form during an aging period.[37−39] These particles, approximately 2.8 nm, are implicated to serve as the nuclei of silicalite-1 particles during the nucleation and crystallization periods. The particle size increases initially from 3 to 5 nm following an Ostwald-ripening mechanism during the induction period after the solution is hydrothermally treated.[36,38] The particles are found to exist during the whole course of crystallization during which the larger particles appear and grow in size through an aggregation−densification mechanism. In this case, the primary particles behave as the nutrient reservoir for the particle growth. The existence of the primary particles is further verified and similar mechanisms are obtained by using in-situ DLS and SAXS techniques.[15,16,18,20,26,27,36,41,43] Analysis of the SAXS data indicates that the primary particles are not spherical.[42,47] The thermochemistry of the crystallization of the precursor solution has also been studied by Navrotsky's group using in-situ calorimetry and pH measurements.[43] The crystallization process

---

* Author to whom correspondence should be addressed. Phone: (979) 845-3492; fax: (979) 845−6446; e-mail: Shantz@che.tamu.edu.

10.1021/jp050733b CCC: $30.25

is initially exothermic and then endothermic. Meanwhile, the solution pH slightly increases initially and then jumps abruptly to a higher value during the crystallization process. The switch from exothermic to endothermic behavior matches the sharp change of the solution pH. A two-step mechanism is proposed to explain the thermochemistry of the solution: prealignment and condensation. Despite all of these studies, there is still contention regarding the detailed mechanism of material nucleation and formation.[22,24,48−51] However, the following points are widely agreed upon: (1) after aging this mixture at room temperature, small colloidal silica particles ($<$5 nm) are present[22,31,37,38,43,47] and (2) after heating this mixture at 368 K for several hours, small ($<$100 nm) particles of silicalite-1 are formed which by all accounts nucleate homogeneously.[35−38] The mechanistic details of this process are still a matter of considerable debate and are the focus of numerous recent and ongoing investigations.

Another metric developed by Zones and Davis that has been used successfully to predict the efficiency of organocations to lead to zeolite formation is the hydrophobicity (C/N^+ ratio) of the organocation, quantified by its partitioning between the organic and aqueous phase of a mixture of water and chloroform.[8] These investigations show that TPA cations have optimized hydrophobic−hydrophilic interactions on the basis of the C/N^+ ratio and partitioning between the organic and aqueous phases. This is consistent with experimental evidence that the organocation is exceptionally efficient in its role as a structure-directing agent (SDA) for silicalite-1.[8] Other tetraalkylammonium cations (methyl, butyl, and pentyl) which are less effective as SDAs for the synthesis of siliceous zeolites have a different partitioning behavior. Moreover, the same trends are followed regardless of the structural symmetry of the organocations.[52,53] Given the wide variety of molecules that can serve as SDAs for zeolite formation, some common features among them include (1) moderate hydrophobicity to silicate species and solvation ability to solvent molecules simultaneously, (2) correlation between the molecule and zeolite pore size/shape, and (3) stability under hydrothermal conditions.

While the TEOS/TPAOH/H_2O system has been intensely studied, there is little work in the literature that has explored how perturbations to this clear solution synthesis impact material formation.[27,28] This information is essential, given the desire to use the insights from silicalite-1 clear solution syntheses to develop a general description of zeolite growth. Recent work from our lab studying SDAs used to make different zeolite phases such as ZSM-12, SSZ-24, and ZSM-11 show that under conditions where silicalite-1 forms rapidly these other phases do not form at all.[54] Rather, silica nanoparticles formed in the solutions, which based on numerous techniques, appear amorphous. The presence of nanoparticles in suspension is consistent with results reported by Fedeyko and co-workers of tetraalkylammonioum hydroxide/silica/water mixtures,[47] and our results, when assembled with their report, indicate that the formation of silica nanoparticles in alkaline solutions containing organocations may be a fairly general phenomena. Motivated by our previous results, the current investigation attempts to answer the following question: How robust is the synthesis of silicalite-1 from clear solutions at 368 K? The current work describes how changes in the SDA structure affect the nucleation and growth of silicalite-1 from clear solutions at 368 K.

Experimental Section

Synthesis of Structure-Directing Agent (SDA). Figure 1 shows the structure-directing agents (SDAs) used in this work.

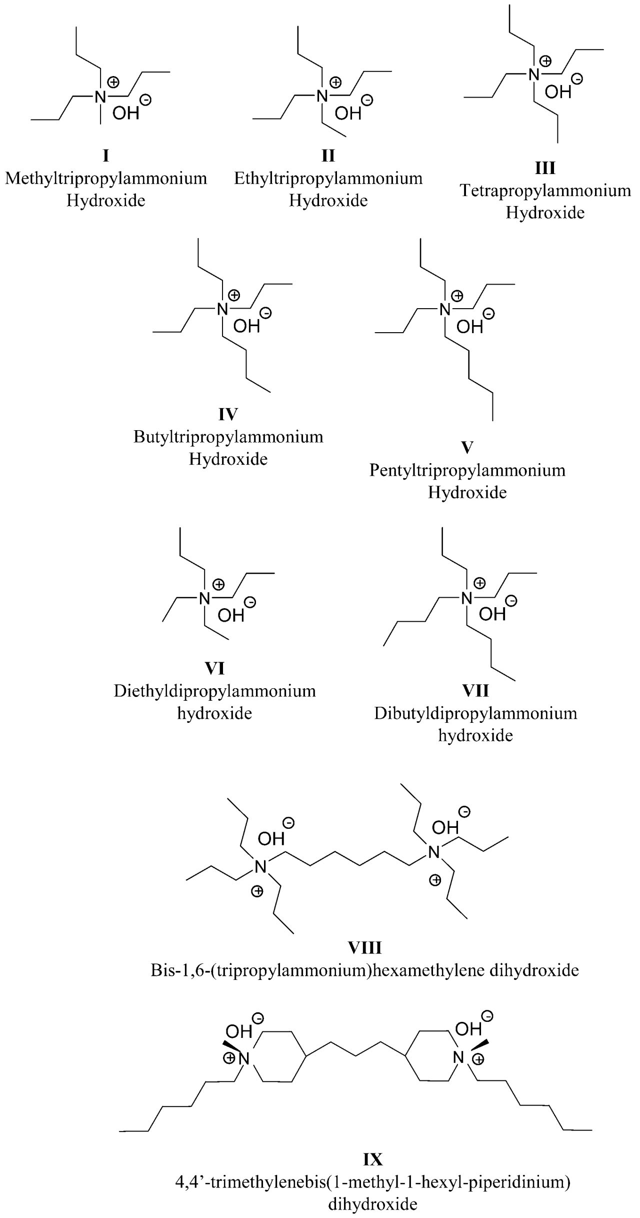

Figure 1. Structure-directing agents (SDAs) used in the current work.

Tetrapropylammonium hydroxide (**III**, Alfa Aesar, 40 wt % in aqueous solution) was used as received. The alkyltripropylammonoium cations ($RN(C_3H_7)_3{}^+OH^-$, R = Me, Et, Bu, and Pe, correspond to **I**, **II**, **IV**, and **V**, respectively) were prepared by reacting the corresponding alkyl halide with tripropylamine. As an example, methyltripropylammonium iodide (**I**) was prepared by the following procedure: 19 mL (0.1 mole) of tripropylamine (Aldrich, 98%) and 200 mL methanol (VWR, ACS grade) were added to a 500-mL round-bottom flask. A second solution containing 24 mL (0.2 mole) of iodomethane (EM Science, $>$98%) and 100 mL methanol was placed in an addition funnel. The iodomethane mixture was subsequently added dropwise to the tripropylamine mixture and the resulting solution was refluxed for 24 h in the absence of light. The solution was then cooled and the methanol was removed by rotary evaporation at reduced pressure. The recovered solids were recrystallized in ethyl acetate (EMD, ACS grade). **II**, **IV**, and **V** were prepared using iodoethane (Aldrich, 99%), iodobutane (Aldrich, 99%), and iodopentane (Aldrich, 98%) as the alkyl halide, respectively. Bis-1,6-(tripropylammonium)hexamethylene diiodide (**VIII**) and 4,4′-trimethylenebis(1-methyl-1-hexyl-piperidinium) diiodide

(**IX**) were made using published procedures.[55,56] Diethyldipropylammonium iodide (**VI**) was prepared as follows: 13.7 mL of dipropylamine (0.1 mol, Aldrich, >99%) and 200 mL methanol (VWR, ACS grade) were added to a 500-mL round-bottom flask. 20.7 g K_2CO_3 (0.15 mole, Aldrich, ACS grade) was added to the mixture and acted as the scavenger of the resulting HI and H_2O during the alkylation reaction. A second solution containing 24 mL of iodoethane (0.3 mole, Aldrich, 99%) and 100 mL methanol was placed in an addition funnel. The iodoethane mixture was subsequently added dropwise to the dipropylamine mixture, and the resulting solution was refluxed for 24 h in the absence of light. The solution was then filtered while it was warm, and the methanol was removed by rotary evaporation at reduced pressure. The recovered solids were recrystallized in ethyl acetate (EMD, ACS grade). Dibutyldipropylammonium iodide (**VII**) was prepared by the same procedure as diethyldipropylammonium iodide (**VI**) except for using iodobutane (0.3 mole, Aldrich, 99%) as the reactant for the alkylation reaction. After removing methanol by rotary evaporation, the recovered solids were recrystallized and rinsed with ether (VWR, ACS grade). The SDAs were ion-exchanged to the hydroxide form using a column containing 200 mL of resin (IONAC NA38, OH^- Form Type L Beads, 1.3 meq/ml, J. T. Baker). The resulting solution was concentrated by rotary evaporation at 333 K. The ion-exchange efficiency and the concentration of the organocation solution were determined by titration with 0.12 N (VWR) HCl solution using Cresol red (Aldrich, indicator grade, 95%) as an indicator. The ion-exchange efficiency was over 95% in all cases.

Zeolite Synthesis. Syntheses were of the composition 1 TEOS:0.36/n $R^{+n}[OH^-]_n$:20 H_2O unless noted otherwise and are given in the figures and text. The following general procedure was followed: 9.2 mL of tetraethyl orthosilicate (Fluka, >99%) was added to a solution of SDA, typically 30−40 wt % in organic (**I**, **II**, and **IV**−**IX**). This mixture was stirred vigorously for 30 min, and any additional water needed was then added. The mixture was then aged for 24 h while mixing at room temperature. Then, half of the solution was placed in a screw cap Teflon container and was heated at 368 K until the solution became opaque as determined by visual inspection. The solids were collected by centrifugation, washed with deionized water, dried, and characterized by powder XRD (Bruker AXS D8). The other half of the solution was used for SAXS in-situ measurements.

Analytical. Powder X-ray diffraction (PXRD) measurements were performed on a Bruker AXS D8 powder diffractometer (Cu Kα radiation) in reflection mode from $2\theta = 4$ to 40° with a step size of 0.03° and 2 s per step. Thermogravimetric analyses (TGA) were performed using a NETZSCH TG 209 with a heating rate of 5 K/min from 303 to 873 K under air environment. The air flow rate was 25 mL/min. The in-situ SAXS experiments were performed on a Bruker NanoSTAR system with a Nonius rotating anode (FR591) and a copper target (1.5417 Å). The anode was operated at 45 kV and 90 mA. The X-ray beam was paralleled by a cross-coupled Göbel mirror and was collimated by three pinholes (750 μm, 400 μm, and 1000 μm in order). The scattering intensity was measured on a two-dimensional multiwire Hi-STAR detector, and the residual direct beam was blocked by a beam stop. The sample-to-detector distances used were 22 and 64 cm, corresponding to a q range of 0.05~0.7 Å^{-1} and 0.02~0.3 Å^{-1} ($q = 4\pi \sin(\theta)/\lambda$, θ is half of the scattering angle, and λ is the wavelength of the incident beam). The exact sample-to-detector distance was determined using a silver behenate standard.

The in-situ SAXS measurements were performed in an electrically heated stage containing a rotating round sample cell. The stage is very similar to that described by de Moor and co-workers.[21] Two clear mica disks (PSI, V1 grade, 15 mm in diameter, 0.15 mm in thickness) were used as windows, with spacing provided by a Teflon ring (McMaster-Carr Co., thickness, 0.5 mm). The cell was heated by two cartridge heaters (Omega Engineering Co., CIR-1014/120 V), and the cell temperature was measured by a K-type thermocouple (Omega Engineering Co., unsheathed T/C) and was controlled by a solid-state relay temperature controller (Omega Engineering Co., CN76031). The in-situ measurements were performed at 368 K and the sampling time was 1.5 h during the reaction. The heating stage was mounted in an Anton Paar HR-PHK sample chamber, and the whole system was purged with helium (>99.99%) several times and then was operated under vacuum (0.1 mbar). The scattered intensity of the particles was calculated on the basis of using water (room temperature and 368 K individually) as the reference material for the background subtraction in data analysis.[15,17] For obtaining the transmission coefficient of the sample, a piece of glassy carbon was inserted into the beam path as a second specimen after each measurement and was taken every three measurements. The transmission coefficients were almost identical during the course of the hydrothermal reaction. Because of the pinhole configuration on the SAXS instrument, no desmearing procedure was required prior to data analysis.

Pair distance distribution functions (PDDFs) were determined from the scattering data using the program GNOM on the basis of the inverse Fourier transform method (IFT).[57−61] For data during the induction period, the particle diameter was obtained using the optimized perceptual criteria introduced by Servgun[62] as well as the Guinier approximation.[63] The radius of gyration obtained from the Guinier approximation is calculated assuming a spherical particle geometry. The values obtained from both approaches were almost identical. For scattering patterns measured following the induction period, the particle size distribution was determined to be bimodal in nature. The diameter of the larger particles was determined from the Guinier approximation, and the particle diameter of the smaller particles was determined from the optimized perceptual criteria within the smaller guessing value ranges. The theoretical fitting, demonstrated as part of the GNOM results (Supporting Information), matched the experimental scattering data in the high q range for this optimized guessing value. However, the low q range data cannot be described using just the small particle population. The growth rate during the crystallization period is determined from the particle diameter as a function of the synthesis duration using linear regression.

Results

Precursor Solutions and Nucleation. Figure 2 shows SAXS measurements of precursor solutions of composition 1 TEOS: 0.36 $RPr_3N^{+n}[OH^-]_n$:20 H_2O that have been aged at room temperature (i.e., not heated). Several things can be noticed from Figure 2. First, all scattering curves exhibit a clear maximum in the log−log plot of I versus q, indicating particle−particle interactions are present ($S(q) \neq 1$). This greatly complicates the analysis as most formalisms (i.e., IFT, Guinier) are not strictly valid except in the dilute solution limit. Moreover, given that for all samples the slope in the high q range is −2, the particles are clearly not spherical. With these points in mind, the values obtained from the Guinier analysis/IFT are approximate; however, clear trends emerge from these analyses.

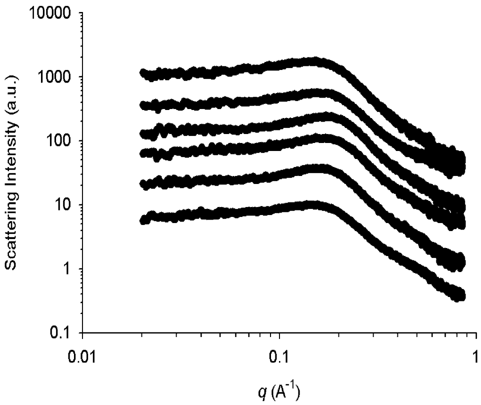

Figure 2. The scattering intensities of silicalite-1 precursor mixtures with the composition of 1 TEOS:0.36/n SDA^{n+}:20 H_2O aged at room temperature for 24 h. From bottom to top, SDA is **I**, **II**, **III**, **IV**, **V**, and **VIII**, respectively. The scattering patterns have been shifted by factors of 2, 10, 15, 40, and 200 for **II**, **III**, **IV**, **V**, and **VIII**, respectively.

Perhaps most noteworthy is that the particles observed in the precursor solutions appear relatively insensitive to the SDA identity for the five TPA-mimics precursor solutions. The particle size, shape, and approximate number density (based on $I(0)$) are quite comparable and are summarized in Table 1 along with the induction period. The main difference between the samples is the induction period or the heating period necessary to observe the formation of larger particles. Given that these larger particles are shown to be silicalite-1 based on WAXS data (see below), it seems reasonable to conclude that silicalite-1 nucleation occurs during the induction period. During the period, the particle diameter decreases to about 2 nm after the solutions were heated for 1.5 h. Thereafter, the particle diameter increases gradually to about 4~5 nm at the end of the induction period and remains almost identical in the following crystallization process. The decrease of particle diameter upon heating, similar to the other zeolite system studied in our group,[54] results in the abrupt increase of the particle number density, implying that the objects formed during the room-temperature aging might dissociate or dissolve under the high-caustic and high-temperature environment. The existence of the primary particles is consistent with published results,[15−17,34,36−38] and the possible role of them will be further discussed below.

Silicalite-1 Growth Kinetics Using Alkyltripropylammonium Cations. In-situ SAXS measurements were performed on silicalite-1 synthesis mixtures containing **I**−**V** with the same composition and reaction conditions to investigate perturbations of SDA structure on silicalite-1 growth kinetics. The solid phase synthesized in the screw cap Teflon container was identified by PXRD as silicalite-1 (Supporting Information). The time-resolved scattering patterns and particle size as a function of the synthesis duration determined by SAXS are shown in Figures 3−7. In all cases, at the end of the induction period a second particle population emerges which are referred to as the “large” particles below. These particles are observed as well as the 5-nm size particles observed during the induction phase. It is also noted here and will be expounded upon in the Discussion section that the number density of 5-nm particles decreases during the crystallization stage as these larger particles grow.

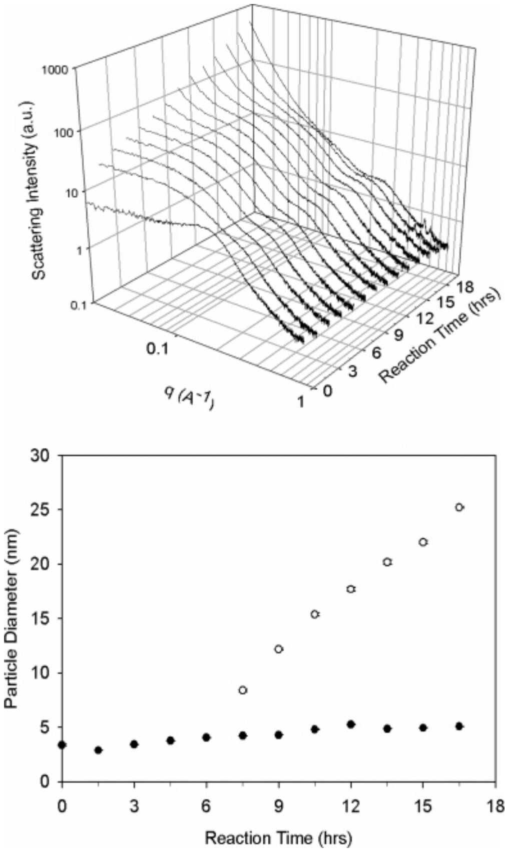

Figure 3. (Top) Time-resolved in-situ SAXS measurements at 368 K for silicalite-1 made with **III** (1 TEOS:0.36 **III**:20 H_2O). (Bottom) Plot of particle size versus reaction time.

Figure 3 shows the SAXS patterns for mixtures containing **III** (TPAOH). After the induction period, the particles begin to grow on the basis of the increase of the scattered intensity at low q ranges (q < 0.05 Å^{-1}). On the basis of the PDDF analysis and preliminary full-profile fitting, it is concluded that there is a bimodal population of particles. This is consistent with dynamic light-scattering measurements and with Schoeman’s in-situ DLS data on this system.[36] (Supporting Information. The minor discrepancy of the particle diameter between DLS and SAXS could be attributed to the differences between ex-situ and in-situ measurements and the fundamentals of the two different techniques.) The particle diameter for the smaller particles is approximately 5 nm during the whole crystallization process (Supporting Information). The size of the large particles determined by the Guinier approximation increases from 4 to 25 nm during the crystallization process, giving a particle growth rate of 1.9 ± 0.1 nm/h. The solution turned hazy after being heated at 368 K for 16.5 h, the time at which Bragg diffraction peaks for the MFI phase at $q \sim 0.54$ and 0.62 Å^{-1} ($2\theta \sim 7.59°$

TABLE 1: Effect of the SDA on the Induction Period

SDA	induction period (h)	particle size (nm)	$I(0)$
methyltripropylammonium hydroxide (**I**)	12.0~13.5	3.6	6.6
ethyltripropylammonium hydroxide (**II**)	10.5~12.0	2.5	7.0
tetrapropylammonium hydroxide (**III**)	6.0~7.5	3.4	6.0
butyltripropylammonium hydroxide (**IV**)	7.5~9.0	2.2	6.6
pentyltripropylammonium hydroxide (**V**)	12.0~13.5	3.7	6.3
bis-1,6-(tripropylammonium)hexamethylene dihydroxide (**VIII**)	12.0~13.5	4.4	4.6

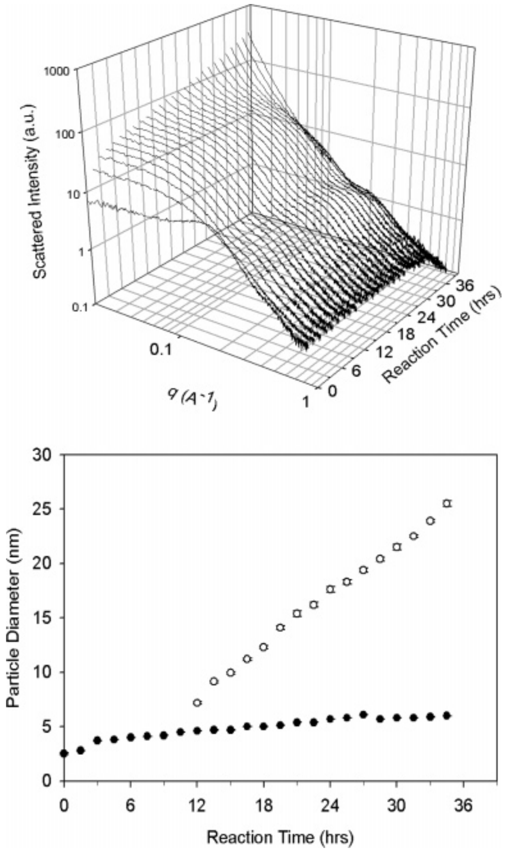

Figure 4. (Top) Time-resolved in-situ SAXS measurements at 368 K for silicalite-1 made with **II** (1 TEOS:0.36 **II**:20 H_2O). (Bottom) Plot of particle size versus reaction time.

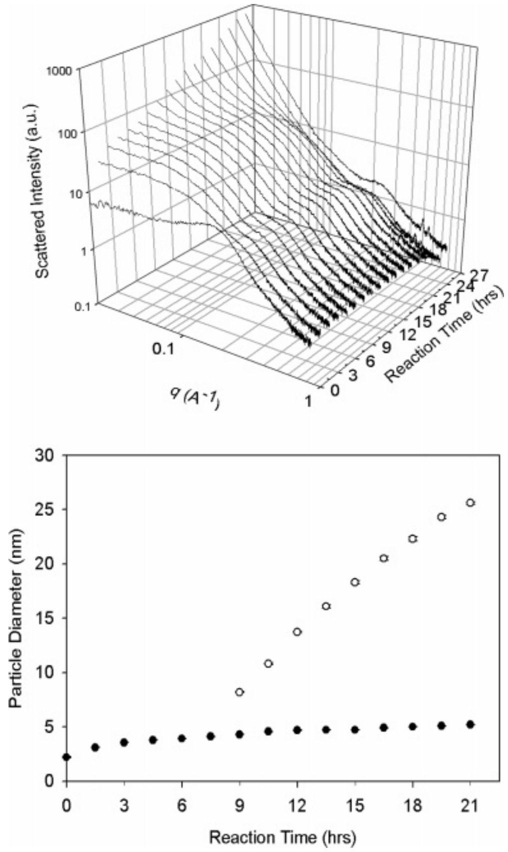

Figure 5. (Top) Time-resolved in-situ SAXS measurements at 368 K for silicalite-1 made with **IV** (1 TEOS:0.36 **IV**:20 H_2O). (Bottom) Plot of particle size versus reaction time.

and 8.72°) are first observed. The slope in the high q range of the scattering patterns is approximately -2 and does not change with the synthesis duration, consistent with nonspherical particles.

Figure 4 shows the time-resolved SAXS data for a synthesis mixture made with **II**, which has one less methylene group than TPA. The evolution of the scattering patterns after the mixture was heated is qualitatively similar to the solution containing **III**, with the notable differences that the induction period is longer and the particle growth rate is slower. The MFI Bragg diffraction peaks do not appear until approximately 36 h, 20 h longer than that of the solution containing **III**. The large particles increase in diameter from 5 to 25 nm during the crystallization period, resulting in a slower growth rate of 0.80 ± 0.02 nm/h. The slope in the Porod regime of the scattering patterns is approximately -2.

A similar result is observed for solutions containing **IV**, which has one more methylene group than TPA. The time-resolved SAXS scattering patterns are shown in Figure 5. The reaction time for the appearance of the Bragg diffraction peaks is 21 h. Within the 12-h crystallization period, the particle diameter increases from 4 to 26 nm, leading to a growth rate of 1.56 ± 0.10 nm/hr. The results in Figures 3−5 clearly show that even a small perturbation to the TPA structure, the addition or removal of one methylene group, leads to an increase in the induction period and a decrease in the silicalite-1 growth rate.

The decrease in the silicalite-1 growth rate becomes more obvious by removing (**I**) or adding (**V**) two methylene groups. The reaction time for the appearance of the Bragg diffraction peaks is approximately 40.5 h and 39 h, respectively (Figures 6 and 7). The particle diameter increases from 4 to 25 nm and from 4 nm to 26 nm during the crystallization period, yielding particle growth rates of 0.70 ± 0.02 and 0.76 ± 0.02 nm/h for mixtures containing **I** and **V**, respectively. Consistent with solutions containing **II** and **IV**, the slopes in the high q range of the corresponding scattering patterns are approximately -2 throughout the syntheses.

Figure 8 summarizes the results above. The figure shows that an approximately parabolic relationship exists between the reaction time for the appearance of Bragg diffraction peaks in the high q range and the particle growth rate versus the number of carbon atoms of the alkyl group of the alkyltripropylammonium cation. For synthesis mixtures containing organocations **I**−**V**, the appearance of Bragg diffraction peaks occurs at a particle diameter of approximately 25 nm. As such, this is used as a semiquantitative metric of zeolite formation and growth. In the context of hydrophobicity, the TPA cation has an intermediate hydrophobic/hydrophilic character ($C/N^+ = 12$) and is located at the extreme positions of both correlations. Making the SDA either more hydrophilic or more hydrophobic leads to a decrease of the growth rate of silicalite-1. These results will be discussed in more detail below in the context of SDA hydrophobicity.

To further probe the effect of SDA geometry on growth kinetics, mixtures containing **VI** and **VII** were studied. Those molecules were chosen as they represent a larger perturbation to the TPA structure as compared to **II** and **IV** individually. However, they have the same C/N^+ ratio as **I** and **V**, correspondingly, which have been demonstrated above to direct the formation of silicalite-1 under these conditions. As such, these organocations were studied to attempt to uncouple SDA hydrophobicity from geometry. In the case of a mixture containing **VI**, the solution became opaque after aging at room temperature for several hours because of the aggregation of

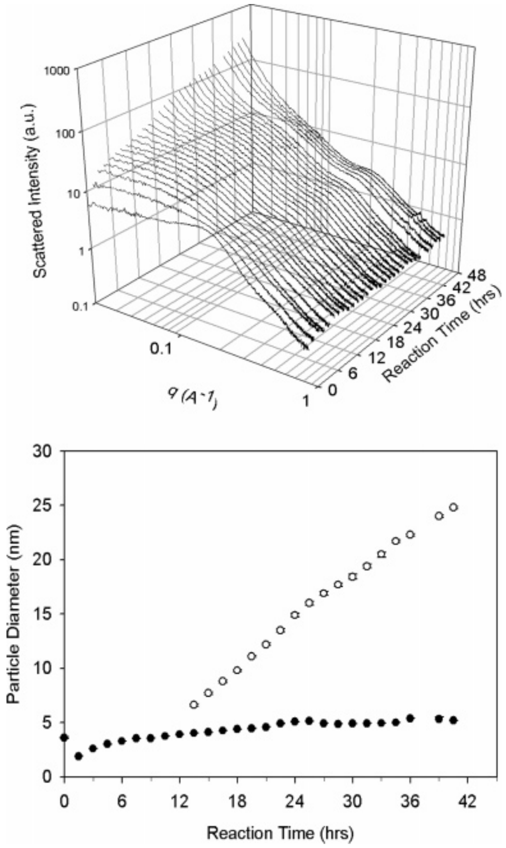

Figure 6. (Top) Time-resolved in-situ SAXS measurements at 368 K for silicalite-1 made with **I** (1 TEOS:0.36 **I**:20 H_2O). (Bottom) Plot of particle size versus reaction time.

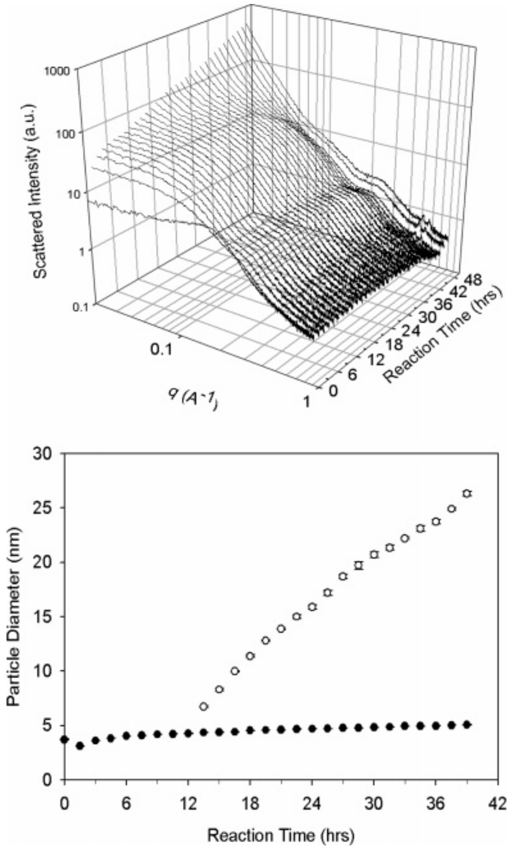

Figure 7. (Top) Time-resolved in-situ SAXS measurements at 368 K for silicalite-1 made with **V** (1 TEOS:0.36 **V**:20 H_2O). (Bottom) Plot of particle size versus reaction time.

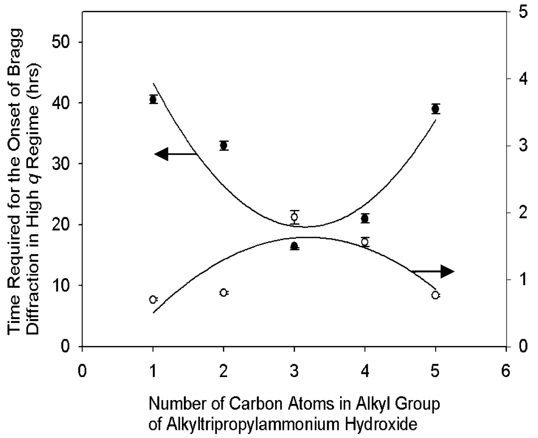

Figure 8. The relationship of the reaction time required for the appearance of the Bragg diffraction in the high q regime (full circle) and the reaction rate (empty circle) versus the number of carbon atoms in the alkyl group of alkyltripropylammonium hydroxide.

silica. The solids were then separated from the mother liquor, and the resulting clear solution was heated at 368 K for 1 week. The clear solution formed solid phases after the hydrothermal treatment. Both the initial solid precipitate and the solids recovered after heating for 1 week at 368 K (recovered by centrifugation) are amorphous silica on the basis of PXRD (Supporting Information). Another attempt to make silicalite-1 at 368 K from the above mixture without removing the precipitated silica also shows that the resulting solid phase is amorphous silica (Supporting Information). Two additional syntheses were performed using **VI** at 433 K for 7 days. One was the precursor solution aged at room temperature with the silica that precipitated included and the other was the clear solution aged at room temperature obtained after removing the precipitate. Both solutions yielded solid phases after 7 days at 433 K. The solids collected from the former solution were identified as a mixture of amorphous silica with a small amount of crystalline solid phase. The solids collected from the latter solution were silicalite-1 on the basis of PXRD (Supporting Information). For the case of synthesis mixtures containing **VII**, the solution became an opaque two-phase solution after aging at room temperature for 24 h. Consistent with the results of solutions containing **VI**, the solution containing **VII** could not stabilize colloidal silica particles. The solid phase collected at the end of hydrothermal reaction was characterized as amorphous silica (Supporting Information). The results show that these organocations cannot stabilize silica nanoparticles in solutions. The reason for this is unclear and is currently being explored. From the above results, although **VI** and **VII**, respectively, have the same C/N$^+$ ratio as **I** and **V**, the solutions cannot direct the formation of silicalite-1, implying that the geometry of the SDA is also essential. That **VI** leads to silicalite-1 formation at 433 K but not at 368 K suggests that the clear solution synthesis of silicalite-1 at 368 K is more sensitive to the SDA structure than to conventional syntheses. This point will be revisited below.

Growth Kinetics Using Other SDAs. The growth behavior of solutions containing **VIII** (TPA-“dimer”) was also studied. This molecule has been shown to make silicalite-1 and has exactly the same C/N$^+$ ratio as TPA.[21,55] Figure 9 shows the SAXS data versus synthesis time. The large particles increase in diameter from 4 to 27 nm over 21 h during the crystallization step, giving a particle growth rate of 1.10 ± 0.01 nm/h. The size of the primary particles and the particle size when the Bragg

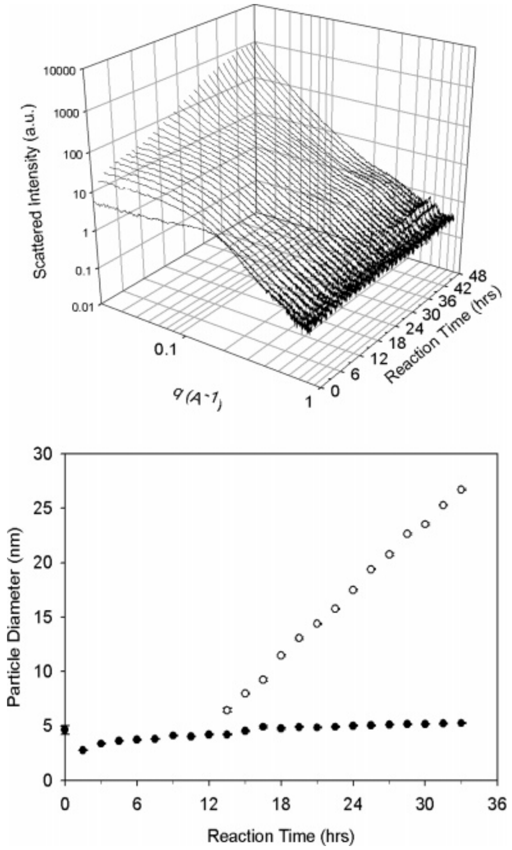

Figure 9. (Top) Time-resolved in-situ SAXS measurements at 368 K for silicalite-1 made with **VIII** (1 TEOS:0.18 **VIII**:20 H_2O). (Bottom) Plot of particle size versus reaction time.

diffraction peaks appear are almost identical to that of syntheses with TPA. In addition, the precursor solution was still transparent at this stage, and it became optically opaque after being heated about 96 h estimated from ex-situ syntheses. The slopes in the high *q* range of the scattering patterns are again approximately -2.

Syntheses were also performed with **IX** which Tsuji and co-workers have shown leads to silicalite-1 formation at 408 K in the presence of alkali cations.[56] This organocation was chosen for investigation since, unlike the cations **I**−**VI**, it is structurally very distinct from TPA. From ex-situ syntheses, amorphous silica was obtained after the solution had been heated at 368 K for 1 week (Supporting Information). This solution behaved similarly to mixtures containing **VI** and **VII** in that silica precipitated from solution after aging overnight at room temperature. **IX** has a C/N^+ ratio equal to 13.5, which is almost identical to **III**, but still cannot form silicalite-1 at 368 K. This result is consistent with the results for organocations **VI** and **VII** that show that the formation of silicalite-1 at 368 K from clear solutions can only tolerate very minor perturbations to the structure of the TPA cation.

Particle Morphology. The morphology of the silicalite-1 particles obtained from syntheses with **I**−**V** and **VIII** after 7 days at 368 K was determined by SEM (Supporting Information). The particle shape appears to be insensitive to the SDA identity, and the size is about 100 nm in diameter for most materials. The particle shape is poorly defined for the solid synthesized from the mixture containing **I**, and the particle size is smaller as compared to the other cases, coincident with the broader Bragg peak width in the PXRD data. The same result is obtained for **VIII**, however, the spherical-like particle shape obtained is different from the elongated morphology observed in previous investigations.[55,64] This is perhaps not surprising given the substantially different synthesis conditions, most notably a much lower synthesis temperature and a higher organocation content. Furthermore, the peak-broadening was also observed by Beck and Davis, attributed to the higher charge carried by the SDA moiety.[55]

Discussion

The results presented above show how the SDA influences the growth kinetics of silicalite-1 from clear solutions at 368 K. This is the first investigation to study this effect on clear solution syntheses at 368 K. As summarized in Tables 1 and 2, the results clearly show that the growth kinetics is strongly sensitive to the SDA as a mere addition (**IV**) or removal (**II**) of a methylene group to one propyl group of TPA leads to a noticeable reduction of the growth rates. The addition (**V**) or removal (**I**) of two methylene groups to one propyl group of TPA has a severe effect on growth kinetics. Perhaps the most surprising result, however, is that either the removal of one methylene group from two of the propyl groups (**VI**) or addition of one methylene group to two of the propyl groups (**VII**) of TPA leads to the inability to form stable silica nanoparticles in suspension and silicalite-1. These results as well as the results with **IX** used by Tsuji and co-workers to make silicalite-1 at 408 K indicate that there is a high degree of SDA specificity necessary for the synthesis of silicalite-1 under the conditions investigated in this report. This is in contrast to syntheses under more conventional conditions (408−433 K), with the presence of alkali where **IX** and **VI** readily form silicalite-1 as do many other organocations.[56,65] What follows below is a discussion placing the results above in the context of existing literature, focusing on three points: (1) the studies by Zones and Davis of SDA hydrophobicity,[8] (2) the possible role of the primary particles during the course of the crystallization period, and (3) comparing the results here to studies at higher temperatures.

The trends observed for the influences of the organocations **I**−**V** on the induction period and growth kinetics are summarized in Tables 1 and 2 and Figure 8 and are consistent with the work performed by Zones and Davis.[8,52,55] Their work shows that organocations with C/N^+ ratio between 11 and 15 can be effective structure-directing agents because of a moderate hydrophobic tendency of the alkyl chain and the water-solvation ability of the molecules.[8] TPA has long been known to be an extremely robust SDA for the formation of silicalite-1; our results here are consistent with that. Also, that the syntheses employing TPA mimics with lower or higher C/N^+ ratios lead to slower growth kinetics is consistent with the argument of hydrophobicity. The decreased growth rates with cations **IV** and **V** could result from the contributions from the hydrophobicity as well as the steric/packing effects in the as-made materials. TGA studies were performed to assess this point (Supporting Information). The organocation content for **III** is approximately 4.2 organocations/unit cell, which is consistent with published results.[45,55] The organocation contents for **IV** and **V** are 4.1 and 2.3 organocations/unit cell, respectively. Since the organocation content of **IV** is close to **III** and that of **V** is approximately equal to **VIII**,[55] the result might indicate that no steric effect exists on the growth kinetics of **IV** but does exist on the growth kinetics of **V**. Hence, the decreased growth rate of **IV** might be totally attributed to the hydrophobicity of the SDA, and the slower growth rate of **V** is due to a combination of the hydrophobicity of the SDA as well as the steric hindrance.

The slower growth rates for syntheses with **I** and **II** could have two origins. One possibility is that given there is likely

TABLE 2: Effect of the SDA on the Crystallization Rate of Silicalite-1

SDA	the reaction time for the appearance of the Bragg diffraction peaks (h)	growth rate during crystallization (nm/h)
methyltripropylammonium hydroxide (**I**)	39.0∼40.5	0.70 ± 0.02
ethyltripropylammonium hydroxide (**II**)	33.0∼34.5	0.80 ± 0.02
tetrapropylammonium hydroxide (**III**)	15.0∼16.5	1.93 ± 0.1
butyltripropylammonium hydroxide (**IV**)	19.5∼21.0	1.56 ± 0.10
pentyltripropylammonium hydroxide (**V**)	37.5∼39.0	0.76 ± 0.02
bis-1,6-(tripropylammonium)hexamethylene dihydroxide (**VIII**)	31.5∼33.0	1.06 ± 0.01

not as good of a “fit” within the silicalite-1 structure as compared to TPA this geometrical effect leads to reduced growth rates. The other possibility is due to hydrophobicity effects. For instance, given their increased hydrophilicity as compared to TPA, it may be that the energy barrier for exchanging the structured water molecules with silicate is higher,[13] resulting in a longer induction period. Moreover, the excess SDA adsorbing on the outer surface of the silica particles[13,47] would lead to stronger electrostatic forces as these cations have a higher effective charge density as compared to TPA.

Consistent with published results,[16,17,19−21,34,36−38] we also observe that small primary particles exist through the course of nucleation and crystallization that are approximately 5 nm in size. That the particle size is independent of the SDA is consistent with previous work by de Moor and co-workers,[21] although the samples here were not heated prior to measurement. After the induction period, two other common features occur in all samples: (1) a second population of particles observed which is silicalite-1 on the basis of the observation of Bragg diffraction peaks and (2) the number density of 5-nm particles decreases as the synthesis proceeds. The latter point was also observed in Schoeman’s in-situ DLS work[36] and Watson and co-workers’ SAXS/SANS results.[41,42] In addition, the $I(0)$ at the end of the induction period decreases with the trend **V** ≅ **IV** ≅ **II** > **III** ≅ **VIII** > **I**, showing that the onset of the crystallization step is independent of the number density of primary particles. These points would seem to indicate that (1) silicalite-1 nucleation occurs during the induction period, (2) the particle growth appears insensitive to the number density of the 5-nm particles, and (3) the 5-nm particles are the silica reservoir for growth, consistent with the mechanism proposed by Schoeman.[34−39] We do not present any results here indicating that zeolite nuclei form directly from the 5-nm particles. ^{29}Si NMR of TAA solutions at room temperature has clearly shown that the primary species in these mixtures are cubic octamer and prismatic hexamer and that it is the pH, not the organocation, which primarily determines speciation in room-temperature mixtures.[66,67] Our results are qualitatively consistent with these observations. However, relating room-temperature speciation to speciation under synthesis conditions is not trivial because of the labile nature of silicate species in solution. Moreover, there is no literature to date that has unambiguously determined silicate speciation in these mixtures under synthesis conditions. Ongoing work in our lab is studying this issue and will be reported elsewhere.

The results for organocations **VI** ($Et_2Pr_2N^+$) and **VII** ($Bu_2Pr_2N^+$) are the most interesting. That **VI** can direct the formation of silicalite-1 at 433 K but not at 368 K suggests that the synthesis of silicalite-1 from clear solutions at 368 K requires highly specific interactions between the SDA and the forming zeolite structure as well as high structural symmetry of the SDA. That removal of the silica precipitate is necessary for the formation of silicalite-1 in the presence of **VI** at 433 K merits further study. However, at the moment definitive statements about this outcome cannot be made as the exact composition of the clear solution is unknown and would lead to a certain level of ambiguity in comparing the results. However, the differences in the growth behavior of **VI** and **IX** between 368 and 433 K support the idea that as the thermal energy of the system is increased silicalite-1 forms more readily in the presence of these SDAs. Along that theme, as the thermal energy of the system is increased, weaker forces (e.g., hydrophobic hydration effects, hydrogen bonding, van der Waals interactions) will become less important as compared to syntheses at lower temperatures.

Conclusion

The SAXS results reported here clearly show that the growth kinetics of silicalite-1 is strongly sensitive to the SDA identity and that small perturbations to the TPA structure can substantially decrease the rate of zeolite formation as manifested by both an increase in the synthesis induction period as well as the crystal growth rate. The results indicate that SDAs with one alkyl group different from TPA can still form silicalite-1 whereas those with two alkyl groups modified cannot. The results indicate that a high degree of SDA structural specificity is necessary to form silicalite-1 from clear solutions at 368 K, something not observed for syntheses at higher temperatures.

Acknowledgment. The authors acknowledge financial support from Texas A&M University and Sabic Americas Inc. The SAXS instruments were purchased from funds obtained under NSF grant CTS-0215838. The authors acknowledge the X-ray Diffraction Facility at Texas A&M University for access to the XRD and SAXS instruments, Professor Eric Simanek (Chemistry, Texas A&M) for access to the TGA instrument, and the Microscopy and Imaging Center (MIC) at Texas A&M for access to the FE-SEM instrumentation. The FE-SEM acquisition was supported by the National Science Foundation under Grant No. DBI-0116835.

Supporting Information Available: PXRD patterns and SEM images of syntheses mixtures with composition 1 TEOS:y SDA:20 H_2O (while SDA = **I**−**V**, $y = 0.36$ and SDA = **VIII**, $y = 0.18$) performed in Teflon containers at 368 K for 1 week, PXRD patterns of syntheses mixture with composition 1 TEOS:y SDA:20 H_2O (while SDA = **VI** and **VII**, $y = 0.36$ and SDA = **IX**, $y = 0.18$) performed in Teflon containers at 368 K for 1 week, PXRD patterns of syntheses mixture with composition 1 TEOS:0.36**VI**:20 H_2O performed in Teflon containers at room temperature for 24 h, PXRD patterns of syntheses mixture with composition 1 TEOS:0.36**VI**:20 H_2O performed in autoclave at 433 K for 1 week, weight loss of the silicalite-1 material prepared by using different organocations as the template with the composition of 1 TEOS:0.36 alkyltripropylammonium hydroxide:20 H_2O under 368 K for 7 days (alkyl group = butyl and pentyl), and the time-resolved scattered intensity at $q = 0$ extracted from GNOM for the precursor solution with the composition of 1 TEOS:0.36/n SDA^{n+}:20 H_2O at 368 K ($n =$

1 for SDA = **I**−**V** and $n = 2$ for SDA = **VIII**). This material is available free of charge via the Internet at http://pubs.acs.org.

References and Notes

(1) Bein, T. *Chem. Mater.* **1996**, *8*, 1636.

(2) Patarin, J.; Lebeau, B.; Zana, R. *Curr. Opin. Colloid. Interface Sci.* **2002**, *7*, 107.

(3) Wirnsberger, G. Y. P. D.; Scott, B. J.; Chmelka, B. F.; Stucky, G. D. *Spectrochim. Acta, Part A* **2001**, *57*, 2049.

(4) Mcmillan, R. A. *Nat. Mater.* **2003**, *2*, 214.

(5) Barrer, R. M. *Hydrothermal Chemistry of Zeolites*; Academic Press: London, 1982.

(6) *Catalysis and Zeolites: Fundamentals and Applications*; Springer: Berlin, 1999.

(7) Breck, D. W. *Zeolite Molecular Sieves: Structure, Chemistry and Use*; Wiley: New York, 1974.

(8) Lobo, R. F.; Zones, S. I.; Davis, M. E. *J. Inclusion Phenom. Mol.* **1995**, *21*, 47.

(9) Szostak, R. *Molecular Sieves - Principles of Synthesis and Identification*; Van Nostrand Reinhold: New York, 1989.

(10) Davis, M. E. *Nature* **2002**, *214*, 813.

(11) Cundy, C. S.; Forrest, J. O.; Plaisted, R. J. *Microporous Mesoporous Mater.* **2003**, *66*, 143.

(12) Burkett, S. L.; Davis, M. E. *J. Phys. Chem.* **1994**, *98*, 4647.

(13) Burkett, S. L.; Davis, M. E. *Chem. Mater.* **1995**, *7*, 1453.

(14) Burkett, S. L.; Davis, M. E. *Chem. Mater.* **1995**, *7*, 920.

(15) de Moor, P.-P. E. A.; Beelen, T. P. M.; Komanschek, B. U.; Diat, O.; van Santen, R. A. *J. Phys. Chem. B* **1997**, *101*, 11077.

(16) de Moor, P.-P. E. A.; Beelen, T. P. M.; van Santen, R. A. *Microporous Mater.* **1997**, *9*, 117.

(17) de Moor, P.-P. E. A.; Beelen, T. P. M.; van Santen, R. A. *J. Appl. Crystallogr.* **1997**, *30*, 675.

(18) de Moor, P.-P. E. A.; Beelen, T. P. M.; Komanschek, B. U.; van Santen, R. A. *Microporous Mesoporous Mater.* **1998**, *21*, 263.

(19) de Moor, P.-P. E. A.; Beelen, T. P. M.; van Santen, R. A.; Tsuji, K.; Davis, M. E. *Chem. Mater.* **1999**, *11*, 36.

(20) de Moor, P.-P. E. A.; Beelen, T. P. M.; van Santen, R. A. *J. Phys. Chem. B* **1999**, *103*, 1639.

(21) de Moor, P.-P. E. A.; Beelen, T. P. M.; van Santen, R. A. *J. Phys. Chem. B* **2000**, *104*, 7600.

(22) Kragten, D. D.; Fedeyko, J. M.; Sawant, K. R.; Rimer, J. D.; Vlachos, D. G.; Lobo, R. F.; Tsapatsis, M. *J. Phys. Chem. B* **2003**, *107*, 10006.

(23) Kirschhock, C. E. A.; Buschmann, V.; Kremer, S.; Ravishankar, R.; Houssin, C. J. Y.; Mojet, B. L.; van Santen, R. A.; Grobet, P. J.; Jacobs, P. A.; Martens, J. A. *Angew. Chem., Int. Ed.* **2001**, *40*, 2637.

(24) Kirschhock, C. E. A.; Ravishankar, R.; Van Looveren, L.; Jacobs, P. A.; Martens, J. A. *J. Phys. Chem. B* **1999**, *103*, 4972.

(25) Kirschhock, C. E. A.; Ravishankar, R.; Jacobs, P. A.; Martens, J. A. *J. Phys. Chem. B* **1999**, *103*, 11021.

(26) Mintova, S.; Olson, N. H.; Senker, J.; Bein, T. *Angew. Chem., Int. Ed.* **2002**, *41*, 2258.

(27) Mintova, S.; Valtchev, V. *Microporous Mesoporous Mater.* **2002**, *55*, 171.

(28) Mintova, S.; Valtchev, V.; Bein, T. *Colloids Surf., A* **2003**, *217*, 153.

(29) Persson, A. E.; Schoeman, B. J.; Sterte, J.; Ottesstedt, J. E. *Zeolites* **1994**, *14*, 557.

(30) Cundy, C. S.; Lowe, B. M.; Sinclair, D. M. *J. Cryst. Growth* **1990**, *100*, 189.

(31) Ravishankar, R.; Kirschhock, C. E. A.; Schoeman, B. J.; Vanoppen, P.; Grobet, P. J.; S. S.; Maier, W.; Martens, J. A.; De Schryver, F. C.; Jacobs, P. A. *J. Phys. Chem. B* **1998**, *102*, 2633.

(32) Ravishankar, R.; Kirschhock, C. E. A.; Knops-Gerrits, P.-P.; Feijen, E. J. P.; Grobet, P. J.; Vanoppen, P.; De Schryver, F. C.; Miehe, G.; Fuess, H.; Schoeman, B. J.; Jacobs, P. A.; Martens, J. A. *J. Phys. Chem. B* **1999**, *103*, 4960.

(33) Ravishankar, R.; Kirschhock, C. E. A.; Verspeurt, F.; Grobet, P. J.; Jacobs, P. A.; Martens, J. A. *J. Phys. Chem. B* **1999**, *103*, 4965.

(34) Schoeman, B. J. *Microporous Mesoporous Mater.* **1998**, *22*, 9.

(35) Schoeman, B. J. *Stud. Surf. Sci. Catal.* **1997**, *105*, 647.

(36) Schoeman, B. J. *Zeolites* **1997**, *18*, 97.

(37) Schoeman, B. J. *Microporous Mesoporous Mater.* **1997**, *9*, 267.

(38) Schoeman, B. J.; Regev, O. *Zeolites* **1996**, *17*, 447.

(39) Schoeman, B. J.; Sterte, J.; Otterstedt, J. E. *Zeolites* **1994**, *14*, 568.

(40) Twomey, T. A. M.; Mackay, M.; Kuipers, H. P. C. E.; Thompson, R. W. *Zeolites* **1994**, *14*, 162.

(41) Watson, J. N.; Iton, L. E.; Keir, R. I.; Thomas, J. C.; Dowling, T. L.; White, J. W. *J. Phys. Chem. B* **1997**, *101*, 10094.

(42) Watson, J. N.; Brown, A. S.; Iton, L. E.; White, J. W. *J. Chem. Soc., Faraday Trans.* **1998**, *94*, 2181.

(43) Yang, S.; Navrotsky, A.; Wesolowski, D.; Pople, J. A. *Chem. Mater.* **2004**, *16*, 210.

(44) Yang, S.; Navrotsky, A. *Chem. Mater.* **2002**, *14*, 2803.

(45) Flanigen, E. M.; Bennett, J. M.; Grose, R. W.; Cohen, J. P.; Patton, R. L.; Kirchner, R. M.; Smith, J. V. *Nature* **1978**, *271*, 512.

(46) Dokter, W. H.; van Garderen, H. F.; Beelen, T. P. M.; van Santen, R. A. *Angew. Chem., Int. Ed. Engl.* **1995**, *34*, 73.

(47) Fedeyko, J. M.; Rimer, J. D.; Lobo, R. F.; Vlachos, D. G. *J. Phys. Chem. B* **2004**, *108*, 12271.

(48) Knight, C. T. G.; Kinrade, S. D. *J. Phys. Chem. B* **2002**, *106*, 3329.

(49) Kirschhock, C. E. A.; Ravishankar, R.; Verspeurt, F.; Grobet, P. J.; Jacobs, P. A.; Martens, J. A. *J. Phys. Chem. B* **2002**, *106*, 3333.

(50) Ramanan, H.; Kokkoli, E.; Tsapatsis, M. *Angew. Chem., Int. Ed.* **2004**, *43*, 4558.

(51) Kirschhock, C. E. A.; Liang, D.; Aerts, A.; Aerts, C. A.; Kremer, S. P. B.; Jacobs, P. A.; Tendeloo, G. V.; Martens, J. A. *Angew. Chem., Int. Ed.* **2004**, *43*, 4562.

(52) Goretsky, A. V.; Beck, L. W.; Zones, S. I.; Davis, M. E. *Microporous Mesoporous Mater.* **1999**, *28*, 387.

(53) Kubota, Y.; Helmkamp, M. M.; Zones, S. I.; Davis, M. E. *Microporous Mater.* **1996**, *6*, 213.

(54) Cheng, C. H.; Shantz, D. F. *J. Phys. Chem. B* **2005**, *109*, 7266.

(55) Beck, L. W.; Davis, M. E. *Microporous Mesoporous Mater.* **1998**, *22*, 107.

(56) Tsuji, K.; Davis, M. E. *Microporous Mater.* **1997**, *11*, 53.

(57) Glatter, O. *J. Appl. Crystallogr.* **1977**, *10*, 415.

(58) Glatter, O. *J. Appl. Crystallogr.* **1979**, *12*, 166.

(59) Glatter, O. *J. Appl. Crystallogr.* **1980**, *13*, 7.

(60) Glatter, O. *J. Appl. Crystallogr.* **1980**, *13*, 577.

(61) Glatter, O.; Kratky, O. *Small Angle X-ray Scattering*; Academic Press: London, 1982.

(62) Svergun, D. I. *J. Appl. Crystallogr.* **1992**, *25*, 495.

(63) Guinier, A.; Fournet, G. *Small-Angle Scattering of X-rays*; John Wiley & Sons: New York, 1955.

(64) Bonilla, G.; Diaz, I.; Tsapatsis, M.; Jeong, H. K.; Lee, Y.; Vlachos, D. G. *Chem. Mater.* **2004**, *16*, 5697.

(65) Goepper, M.; Li, H.-X.; Davis, M. E. *Chem. Commun.* **1992**, 1665.

(66) Knight, C. T. G.; Syvitski, R. T.; Kinrade, S. D. *Stud. Surf. Sci. Catal.* **1995**, *97*, 483.

(67) Kinrade, S. D.; Knight, C. T. G.; Pole, D. L.; Syvitski, R. T. *Inorg. Chem.* **1998**, *37*, 4272.